STABILIZATION OF THE LOWER HYBRID DRIFT INSTABILITY BY RESONANT ELECTRONS

by

Yu-Jiuan Chen, William M. Nevins

and Charles K. Birdsall

Memorandum No. UCB/ERL M81/72

16 September 1981

ELECTRONICS RESEARCH LABORATORY

College of Engineering
University of California, Berkeley
94720

STABILIZATION OF THE LOWER HYBRID DRIFT INSTABILITY BY RESONANT ELECTRONS

Yu-Jiuan Chen

Electronics Research Laboratory

University of California, Berkeley, California 94720

William M. Nevins

Lawrence Livermore National Laboratory

University of California, Livermore, California 94550

Charles K. Birdsall

Electronics Research Laboratory

University of California, Berkeley, California 94720

ABSTRACT

The lower hybrid drift instability was studied with a two dimensional electrostatic simulation code. Simulations showed good agreement of the measured local growth rates and frequencies with the results of local theory during the early stage of wave growth. At later times nonlocal effects become important, and a coherent mode structure develops. This normal mode was observed to propagate up the density gradient.

At zero plasma beta and zero electron temperature, we found that the lower hybrid drift instability is stabilized by the local current relaxation due to both ion quasilinear diffusion and electron $\vec{E}\times\vec{B}$ trapping which causes electron heating to occur.

I. INTRODUCTION

In the past several years the lower hybrid drift instability[1] has attracted considerable interest within the plasma physics community, since it is likely that this mode limits plasma confinement in theta pinches and field- reversed configurations. This instability was simulated by two of the authors previously in the low drift velocity regime ($v_d \ll v_{ti}$) by using an one-dimensional, electrostatic particle hybrid code[2] . $v_d = v_{de} - v_{di}$ is the difference between the electron and ion cross-field velocities, and $v_{ti} = (T_i/m_i)^{1/2}$ is the ion thermal velocity. It was found that if the relative electron-ion drift velocity is kept constant in time, which models a finite beta plasma[3] , ion trapping causes saturation of the instability. If this drift is allowed to decrease consistent with momentum balance, which is related to the zero beta plasma case, then saturation is due to current relaxation[4,5] . Two dimensional particle simulations of this instability with a finite plasma beta value for large drift velocities ($v_d \gg v_{ti}$) were performed by Winske and Liewer[6] . Ion trapping was also the saturation mechanism in their simulations. Our object in this paper is to study the lower hybrid drift instability at zero plasma beta in the low drift velocity regime with both a two dimensional electrostatic simulation code and a nonlocal theory.

A slab configuration is used with a density gradient in x (Fig. 1). In the initial Vlasov equilibrium, the ion pressure gradient balances the zeroth order ambipolar electric force on the ions. Since the characteristic frequency of the lower hybrid drift instability is much greater than the ion cyclotron frequency, the ions may be treated as unmagnetized particles.

Simulations show good agreement of the measured local growth rates and frequencies with the results of local theory[4] during the early stage of wave growth when the wave energy is mostly localized at the region x_0 where electrons have the largest $\vec{E} \times \vec{B}$ drift velocity. After a transit time, i.e., the time for the wave pocket traveling at the group velocity to across the whole system along the density gradient. Nonlocal effects become important and a coherent mode structure develops. This normal mode is observed to propagate from x_0 across the zeroth order density gradient to regions where the electron drift velocity v_E equals the wave phase velocity (ω/k_y) , and to be damped by these resonant electrons. v_E is electron $\vec{E} \times \vec{B}$ drift velo-

city due to the ambipolar electric field.

At zero plasma beta and zero electron temperature, we found that the lower hybrid drift instability is stabilized by current relaxation due to both ion quasilinear diffusion[4,5] and electron $\vec{E}\times\vec{B}$ trapping[7]. According to Drake and Huba[7], electrons with a drift velocity (including both the zeroth order and the perturbed $\vec{E}\times\vec{B}$ drift velocity in the y direction) which is greater than or equal to the wave phase velocity, are in resonance with the wave, and can become trapped. This electron $\vec{E}\times\vec{B}$ trapping was observed in the simulation. The trapping caused local current relaxation by modificating of the electron density profile. The neighborhood of the point where the electrons have the greatest relative drift velocities is the most unstable region according to local theory. In this region, we found that the current relaxes by modification of the ion velocity distribution function as well.

In Sec. II, a description of the simulation model and initial equilibrium is presented. Comparisons of observed linear, local properties of the lower hybrid drift instability with linear local theory are made and given in Sec. IIIA. Section IIIB is devoted to nonlocal effects of the lower hybrid drift instability. A nonlocal theory is presented. Current relaxation caused by ion quasilinear diffusion and electron $\vec{E}\times\vec{B}$ trapping is discussed in Sec. IV. Conclusions are given in Sec. V.

II. SIMULATION MODEL AND INITIAL EQUILIBRIUM

In our simulations, a slab configuration was assumed and the Vlasov equilibria are functions of x only. All the zeroth order drift velocities are in the y direction and the uniform magnetic field is in the z direction. The simulations were carried out in the x-y plane by using the two-dimensional electrostatic, fully nonlinear particle code, EZOHAR[8,9]. In EZOHAR, the boundary conditions along x are inversion symmetry[9] at the high density side and a reflecting boundary at the low density side. The simulation system is periodic in the y direction.

Since the mode frequency of the lower hybrid drift instability is much higher than the ion cyclotron frequency, ions are assumed to be unmagnetized. In the equilibrium, it was assumed

that the ion pressure force is balanced by the zeroth order ambipolar electric force. From the Vlasov equation, the ion distribution function is then only a function of energy H_i where

$$H_i = m_i v^2/2 + e\phi(x) \quad . \tag{1}$$

Let the ion distribution function $f_i(H_i)$ be exponential, as

$$f_i(H_i) = C_i \exp[(-m_i v^2/2 + e\phi(x))/T_i] \quad . \tag{2}$$

Rewrite Eq. (2) as a product,

$$f_i(H_i) = n_i(x)\, g_i(v) \quad . \tag{3}$$

Here

$$g_i(v) = C_i \exp(-m_i v^2/2T_i) \tag{4}$$

is the Maxwellian distribution. The ion density profile is

$$n_i(x) = n_0 \exp\left[-e\frac{\phi(x)-\phi(0)}{T_i}\right] \quad . \tag{5}$$

n_0 is the ion density at $x=0$.

Similarly, the electron equilibrium distribution function is a function of two electron invariants: energy,

$$H_e = m_e v^2/2 - e\phi(x) \tag{6}$$

and the guiding center position

$$X = x - v_y/\omega_{ce} \quad . \tag{7}$$

Let the electron distribution function $f_e(H_e, X)$ be given as

$$f_e(H_e, X) = F(X) \exp(-m_e v^2/2 + e\phi)/T_e \quad . \tag{8}$$

For a small electron gyroradius and a slowly varying ambipolar field, i.e., $a_e(d\phi/dx)\phi^{-1} \ll 1$, the electric potential can be expanded around the guiding center position as

$$\phi(x) = \phi(X) + \Delta x \frac{d\phi}{dx}\Big|_X + \ldots\ldots \tag{9}$$

where

$$\Delta x = x - X = v_y/\omega_{ce} \tag{10}$$

is the electron displacement from its guiding center. Therefore, Eq. (9) becomes

$$\phi(x) = \phi(X) - v_y E(X)/\omega_{ce} \quad . \tag{11}$$

Substitute Eq. (11) into Eq. (8) and rewrite Eq. (8) as

$$f_e(H_e,X) = F(X)\exp\left\{\frac{m_e v_E^2(X)/2+e\phi(X)}{T_e}-\frac{m_e}{2T_e}\left[v_x^2+\left(v_y-v_E(X)\right)^2\right]\right\}$$

$$=N_e(X)\,g_e(v) \tag{12}$$

where $N_e(X)$ is the electron guiding center density profile and

$$g_e(v) = C_e\exp\left\{-\frac{m_e}{T_e}\left[v_x^2+\left(v_y-v_E(X)\right)^2\right]\right\} \tag{13}$$

is the electron drifting Maxwellian distribution.

From the Poisson equation,

$$\frac{dE(x)}{dx} = 4\pi e[n_i(x)-n_e(x)] \ , \tag{14}$$

and Eq. (5), $n_i(x)$ and $n_e(x)$ can be determined by choosing an appropriate $E(x)$, where $n_e(x)$ is the electron particle density. The E field with the form

$$E(x) = -2E_0\tanh(x/L)\,\mathrm{sech}(x/L) \ , \tag{15}$$

which gives a peak value as $-E_0$ at $x=x_0=L\sinh^{-1}(1)$, was chosen in our simulations. Therefore, the ion density profile is

$$n_i(x) = n_0\exp\left[-\frac{2eE_0L}{T_i}\tanh^2(x/L)\right] \ . \tag{16}$$

The electron density n_e can be obtained by substituting Eqs. (15) and (16) into Eq. (14). According to Eq. (12), electrons have to be loaded by following the electron guiding center density profile $N_e(X)$ which can approximately be expressed in terms of n_e as

$$N_e(X) \approx n_e(x)+\frac{a_e^2}{4}\frac{d^2n_e}{dx^2}\Big|_x \ , \tag{17}$$

for $a_e\frac{dn_e}{dx}/n_e<<1$. Hence, the electron guiding center density $N_e(X)$ is determined once $E(x)$ has been specified. Equilibrium profiles of the normalized ion density $n_i(x)/n_0$ and the relative electron-ion drift velocity $v_E(x)$ are shown in Figs. 2(a) and (b).

There was a 64×64 spatial grid in the simulated system. The dimension in x was $42.43\lambda_{Di}$ and that in y was $44.43\lambda_{Di}$, where λ_{Di} is the ion Debye length. Time step $\omega_{pe}\Delta t=0.2$ was

chosen and 32768 particles were used for each species. The mass ratio m_i/m_e in the simulation was 100 and $\omega_{pe}^2/\omega_{ce}^2=1$, where ω_{pe} and ω_{ce} are electron plasma and cyclotron frequencies, respectively. Ty,pically v_{E_0}/v_{ti} was varied from 0.6 to 3.6, where $v_{E_0}=cE_0/B$ is the maximum electron $\vec{E}\times\vec{B}$ drift velocity located at $x=x_0$.

III. SIMULATION RESULTS AT LINEAR STAGE

A. Local Effects

Figure 3 shows a history plot of the simulation electrostatic energy of a single Fourier mode at x_0 , where electrons have the largest $\vec{E}\times\vec{B}$ drift velocities. According to local theory[7] , the region near x_0 is the most unstable area. The theoretical local growth rate is drawn as a straight line . Simulation local growth rates and frequencies for different modes were measured and compared with the theoretical results in the largest drift velocity region, as shown in Figs. 4(a)-(d) for $v_{E_0}/v_{ti}=0.6$, 0.9, 1.2 and 3.6, respectively. The figure shows good agreement of simulations with local theory during the early stage of wave growth.

B. Nonlocal Effects

From the simulations, it was found that nonlocal effects become important at later times, and a coherent mode structure develops along x as shown in Fig. 5. Figure 6 shows a snapshot of a potential contour plot from a single mode simulation, i.e., except for the $k_y=0$ mode, only one Fourier component in k_y of electric potential was used to push the particles. The $k_y=0$ mode is necessary in order to allow an ambipolar electric field due to the charge separation. Note that no Fourier transform of electric potential was made in the x direction. Therefore, all possible k_x modes existed in our simulations. From Fig. 6, we found that plasma system can be divided into three regions. At the most unstable region where electrons have the largest $\vec{E}\times\vec{B}$ drift velocities, the wave vector $\vec{k}$ was observed in the y direction as predicted by local theory. The plasma has larger density in the region left of the maximum $\vec{E}\times\vec{B}$ drift velocity point. It was observed that the normal mode of the lower hybrid drift instability propagates toward higher density with a mean wave vector $\vec{k}\approx k_y(-\vec{e}_x+\vec{e}_y)$ that is, with a $k_x\approx -k_y$. In the

second region, the lower hybrid drift wave was found to travel down the density gradient. These phenomena may be explained by the following argument.

We have found the governing eigenmode equation for the lower hybrid drift instability in a slab geometry to be[10]

$$\frac{\partial^2\phi_{k_y}(x)}{\partial x^2}+\frac{\omega_{pe}^2/\omega_{ce}^2}{1+\omega_{pe}^2/\omega_{ce}^2}\frac{\partial N_e(x)/\partial x}{N_e(x)}\frac{\partial\phi_{k_y}(x)}{\partial x}-\left[k_y^2+\frac{1}{\lambda_{Di}^2(x)}\frac{1}{1+\omega_{pe}^2/\omega_{ce}^2}\frac{\omega}{\omega-k_y v_E(x)}\right]\phi_{k_y}(x)$$
$$-i\sqrt{\frac{\pi}{2}}\frac{1}{4\pi\lambda_{Di}^2(x)}\frac{1}{1+\omega_{pe}^2/\omega_{ce}^2}\frac{\omega}{|k|v_{ti}}\phi_{k_y}(x)=0 \qquad (18)$$

for $v_E(X)\ll v_{ti}$. $\phi_{k_y}(x)$ is a Fourier component in k_y of the perturbed electrostatic potential. Let

$$\phi_{k_y}(x)=\psi(x)\exp[-\int\alpha(x)\,dx] \ , \qquad (19)$$

and put this into Eq. (18) to obtain the standard form

$$\frac{\partial\psi(x)}{\partial x^2}-Q(k_y,\omega,x)\psi(x)=0 \ , \qquad (20)$$

where

$$Q(k_y,\omega,x)=Q_r(k_y,\omega,x)+iQ_i(k_y,\omega,x) \ , \qquad (21)$$

$$Q_r(k_y,\omega,x)=k_y^2+\frac{1}{2}\frac{\partial^2}{\partial x^2}\ln(1+\omega_{pe}^2/\omega_{ce}^2)+\frac{1}{4}\left[\frac{\partial}{\partial x}\ln(1+\omega_{pe}^2/\omega_{ce}^2)\right]^2 \qquad (22)$$
$$+\frac{1}{\lambda_{Di}^2(x)}\frac{1}{1+\omega_{pe}^2/\omega_{ce}^2}\frac{\omega}{\omega-k_y v_E(x)} \ ,$$

and

$$Q_i(k_y,\omega,x)=\sqrt{\frac{\pi}{2}}\frac{1}{\lambda_{Di}^2(x)}\frac{1}{1+\omega_{pe}^2/\omega_{ce}^2}\frac{\omega}{|k|v_{ti}} \ . \qquad (23)$$

The perturbed electric potential is related to ψ through

$$\phi(x,y,t)=\left[1+\omega_{pe}^2(x)/\omega_{ce}^2\right]^{-1/2}\psi(x)\,e^{i(k_y y-\omega t)} \ . \qquad (24)$$

The Fourier component $\phi_{k_y}(x)$ of the perturbed potential, was solved for numerically by using Eq. (20), and is shown in Fig. 5(b). Comparing the simulation result Figs. 5(a) with 5(b), we see that the normal mode structures from simulations and theory are very similar.

In order to understand the contribution of resonant electrons and ions, we now derive an

equation of the wave energy flow. Assume ω_0 is the eigenfrequency of the equation

$$\frac{\partial^2\psi}{\partial x^2} - Q_r(k_y,\omega,x)\psi(x) = 0 \tag{25}$$

where $\omega_0=\omega_r+i\gamma$ and $\gamma\to 0$. Expanding $Q(k_y,\omega,x)$ around ω_0 gives

$$Q(k_y,\omega,x) = Q(k_y,\omega_0,x) + \frac{\partial Q}{\partial\omega}(k_y,\omega_0,x)(\omega-\omega_0) = Q_0 + iQ_0'\frac{\partial}{\partial t} \ , \tag{26}$$

where $Q_0=Q(k_y,\omega_0,x)$, $Q_0'=\frac{\partial Q}{\partial\omega}(k_y,\omega_0,x)$, and $\omega-\omega_0$ is replaced by $i\partial/\partial t$. Substituting Eq. (26) into Eq. (20), we get

$$\frac{\partial^2\psi}{\partial x^2} - Q_0\psi - iQ_0'\frac{\partial\psi}{\partial t} = 0 \ . \tag{27}$$

Multipling Eq. (27) with ψ^* gives

$$\psi^*\frac{\partial^2\psi}{\partial x^2} - Q_0|\psi|^2 - iQ_0'\psi^*\frac{\partial\psi}{\partial x} = 0 \ . \tag{28}$$

Subtracting Eq. (28) from its complex conjugate, we obtain

$$\mathrm{Re}(Q_0')\frac{\partial|\psi|^2}{\partial t} + 2\mathrm{Im}\,Q_0|\psi|^2 + i\frac{\partial}{\partial x}(\psi^*\frac{\partial\psi}{\partial x} - \psi\frac{\partial\psi^*}{\partial x}) + i\mathrm{Im}\,Q_0(\psi^*\frac{\partial\psi}{\partial t} - \psi\frac{\partial\psi^*}{\partial t}) = 0. \tag{29}$$

The physical meanings of those four terms in the above equation are the rate of wave energy change, the source or sink of wave energy, the flux of the wave energy, and the frequency shift due to growth or damping of the wave, respectively. The ratio of the second term to the first term gives the growth or damping rate. Let us concentrate on the second term only. According to Eqs. (21)-(23), $\mathrm{Im}\,Q_0$ can be expressed as

$$\mathrm{Im}\,Q_0 = \frac{1}{\lambda_{Di}(x)}\frac{1}{1+\omega_{pe}^2/\omega_{ce}^2}\left\{\lim_{\gamma\to 0}\left[-\frac{\gamma k_y v_E(x)}{\left(\omega_r - k_y v_E(x)\right)^2+\gamma^2} + \sqrt{\frac{\pi}{2}}\frac{\omega_r}{|k|v_{ti}}\right]\right\}$$

$$= \frac{1}{\lambda_{Di}(x)}\frac{1}{1+\omega_{pe}^2/\omega_{ce}^2}\left[-\pi k_y v_E(x)\delta\left(\omega_r - k_y v_E(x)\right) + \sqrt{\frac{\pi}{2}}\frac{\omega_r}{|k|v_{ti}}\right] \ . \tag{30}$$

The second term in Eq. (30) represents the resonant ions which drive the lower hybrid drift instability, a negative energy wave, as predicted by local linear theory. The delta function in the first term represents resonant electrons whose $\vec{E}\times\vec{B}$ drift velocity equals to the y phase velocity of the wave. The opposite sign of the first term from that of the second term shows

that those resonant electrons have stabilizing effects on the lower hybrid drift instability. Suppose that the plasma has a density profile similar to the density profile shown in Fig. 2(a), and the electron $\vec{E}\times\vec{B}$ drift velocity as function of x is similar to the drift velocities in Fig. 2(b); then there are two places in the system that electron drift velocities equal the y phase velocity of the wave excited at the most unstable region. One resonant point is near the center of the plasma ($x\approx 1.2$ in Fig. 2(b)), and another is at the outer edge of the plasma (outside of our simulation system in Fig. 2(b)). Therefore, when the lower hybrid drift wave is excited at the largest drift velocity region, the wave packet will travel in x to these two electron resonant points, where it dumps wave energy into the resonant electrons.

IV. SATURATION MECHANISMS

Saturation mechanisms of the lower hybrid drift instability in a uniform magnetic field at zero plasma beta and zero electron temperature were studied. Simulation results show that the lower hybrid drift instability is stabilized by current relaxation which is due to both ion quasilinear diffusion and electron $\vec{E}\times\vec{B}$ trapping. According to local theory, the neighborhood of the point where electrons have the largest relative drift velocities is the most unstable region. In this region, we found that the current relaxes by modification of the ion velocity distribution function. Figures 7(a) and (b) are ion velocity distribution functions, averaged in x over the whole system, versus v_x and v_y , respectively, for $v_{E_0}/v_{th}=0.6$ from a single mode simulation. Small modifications of the ion distribution function occurred after saturation. The slight flattening around a small negative v_x in Fig. 7(a) shows that the wave propagates in the negative x direction. Similarly, Fig. 7(b) shows that the wave also propagates in the positive y direction. Hence, the lower hybrid drift mode propagates up the density gradient. For a larger drift velocity, the lower hybrid drift wave is more localized around the most unstable region. Figures 8(a) and (b) are ion distribution functions averaged over x between $x=21\Delta x$ and $x=32\Delta x$, which is the most unstable region in the system, for $v_{E_0}/v_{th}=3.6$ from a single mode simulation, where Δx is the grid cell size and there are 64 grids across the system in x. Larger modifications of the ion velocity distribution functions are shown in this case.

According to Drake and Huba[7] , when the electron drift velocity, which includes both the zeroth order and the perturbed $\vec{E}\times\vec{B}$ drift velocity in the y direction, is equal to or greater than the wave phase velocity, electrons are in resonance with the wave. This electron $\vec{E}\times\vec{B}$ trapping was observed in our simulations in the range that v_{E_0}/v_{ti}=0.6 to 3.6 . Figure 9 gives a snapshot of an electron density contour plot for v_{E_0}/v_{ti}=0.9 from a single mode simulation. The similarity of the electron density contour and the electric potential contour given in Fig. 6 shows that electrons move along constant potential contours, and electrons around x=1.2 are trapped by the wave. This electron $\vec{E}\times\vec{B}$ trapping causes current relaxation by local flattening of the density profile around the trapping region as shown in Fig . 10 at $x\approx$1.2 and Fig. 11 at $x\approx$0.8 for v_{E_0}/v_{ti}=0.9 and 3.6 . The other flattening of electron density profiles in Fig. 10 at $x\approx$3.0 and Fig. 11 at $x\approx$2. are due to the ion quasilinear modifications in the most unstable regions. Figures 12(a) and (b) show electron phase space (v_y versus x) for v_{E_0}/v_{ti}=0.9 and 3.6 . The initial electron temperature is zero and the initial drift velocities are given by the solid curves. We found that the averaged electron current was reduced after saturation of the wave. After subtracting the guiding center velocity from the electron total velocity, electron heating (shown in Fig. 13) due to electron $\vec{E}\times\vec{B}$ trapping was observed starting around the electron resonant region ($x\approx$1.2 as shown in Figs. 2(b) and 5) and gradually spreading to the whole plasma system.

Finally, the simulated saturation levels are compared with saturation levels predicted by both ion quasilinear diffusion theory[4,5] and electron $\vec{E}\times\vec{B}$ trapping[7] . The local approximation was used in the ion quasilinear diffusion theory which gives the saturation level due to current relaxation as

$$\frac{\epsilon}{nT_i} = \frac{1}{8}\frac{m_e}{m_i}\frac{1}{1+\omega_{pe}^2/\omega_{ce}^2}\left(\frac{v_E}{v_{ti}}\right)^2 , \tag{31}$$

where $\epsilon=<\delta E^2>/8\pi$. Assuming that the most unstable mode is dominant, Eq. (31) can be rewritten as

$$\frac{e\delta\phi}{T_i} = \frac{1}{2}\left(\frac{m_e}{m_i}\right)^{1/2}\frac{v_E}{v_{ti}} , \tag{32}$$

where $\delta\phi$ is the perturbed electrostatic potential. Assuming that the zeroth order ambipolar electric field vanishes and setting the perturbed $\vec{E}\times\vec{B}$ drift velocity equal to the wave phase velocity, the saturation level of the most unstable mode due to electron $\vec{E}\times\vec{B}$ trapping is given as

$$\frac{e\delta\phi}{T_i} = \frac{1}{2}\left(\frac{m_e}{m_i}\right)^{1/2}\frac{v_E}{v_{ti}}\left(1+\omega_{pe}^2/\omega_{ce}^2\right)^{-1/2}\frac{k_y}{k_x} \quad . \tag{33}$$

In Fig. 14, Eqs. (32) and (33) are plotted for $m_i/m_e=100$, $\omega_{pe}^2/\omega_{ce}^2=1$, and $k_x=k_y$. Simulation levels are smaller than both the theoretically predicted levels by roughly a factor of two; this could be due to the combination of ion quasilinear diffusion and electron $\vec{E}\times\vec{B}$ trapping occurred in our simulations. From Fig. 14, our simulated data gives

$$\frac{e\delta\phi}{T_i}\approx\frac{1}{4}\left(\frac{m_e}{m_i}\right)^{1/2}\frac{v_E}{v_{ti}} \quad . \tag{34}$$

Furthermore, $v_E-\omega/k_y$ varies and even goes to zero at the electron resonant point in our simulations, where v_E is only the zeroth order $\vec{E}\times\vec{B}$ drift velocity. This could cause electron $\vec{E}\times\vec{B}$ trapping occurring at a lower level.

V. CONCLUSIONS

Two-dimensional electrostatic particle simulations of the lower hybrid drift instability in the low drift velocity regime have been presented. Simulations show good agreement of the measured local growth rates and frequencies with the results of local theory during the early stage of wave growth. At later times nonlocal effects become important, and a coherent mode structure develops. We found that the lower hybrid drift instability is stabilized by the local current relaxation due to both ion quasilinear diffusion at the most unstable region and electron $\vec{E}\times\vec{B}$ trapping around the electron resonant region. Electron heating due to electron $\vec{E}\times\vec{B}$ trapping was observed at the electron resonant region.

ACKNOWLEDGMENTS

We are very grateful to Dr. B. I. Cohen for his helpful conversations.

This research was partially supported by the Office of Naval Research Contract No. N00014-77-C-0578 (Berkeley), and in part by the Department of Energy under Contract No. W-7405-ENG-48 (Livermore). The computational portion of this work was supported by the National Magnetic Fusion Energy Computer Center at Lawrence Livermore National Laboratory.

REFERENCES

1. N. A. Krall and P. C. Liewer, "Low-Frequency Instabilities in Magnetic Pulses", Phys. Rev. A4, 2094 (1971).

2. Yu-Jiuan Chen and C. K. Birdsall, "Lower-Hybrid Drift Instability Saturation Mechanisms in One-Dimensional Simulations", Memorandum No. UCB/ERL M80/40 (1980), accepted by Phys. Fluids.

3. J. D. Huba, J. F. Drake and N. T. Gladd, "Lower-Hybrid Drift Instability in Field Reversed Plasma", Phys. Fluids 23, 552 (1980).

4. R. C. Davidson and N. T. Gladd, "Anomalous Transport Properties Associated with the Lower-Hybrid- Drift Instability", Phys. Fluids 18, 1327 (1975).

5. R. C. Davidson, "Quasi-linear Stabilization of the Lower-Hybrid-Drift Instability", Phys. Fluids 21, 1375 (1978).

6. D. Winske and P. C. Liewer, "Particle Simulation Studies of the Lower Hybrid Drift Instability", Phys. Fluids 21, 1017 (1978).

7. J. F. Drake and J. D. Huba, "Saturation and Transport by the Lower Hybrid Drift Instability in Two Dimensions", Sherwood Theory Meeting, Austin, Texas (1981).

8. A. B. Langdon and B. F. Lasinski, "Methods in Computational Physics", (Academic Press, N. Y., N. Y., 1976), Vol. 16, pp. 327-361.

9. W. M. Nevin, Y. Matsuda and M. J. Gerver, "Plasma Simulations Using Inversion Symmetry as a Boundary Condition", J. Comp. Phys. 39, 266 (1981).

10 Yu-Jiuan Chen and W. M. Nevins, "Nonlocal Theory of the Lower Hybrid Drift Instability", in preparation.

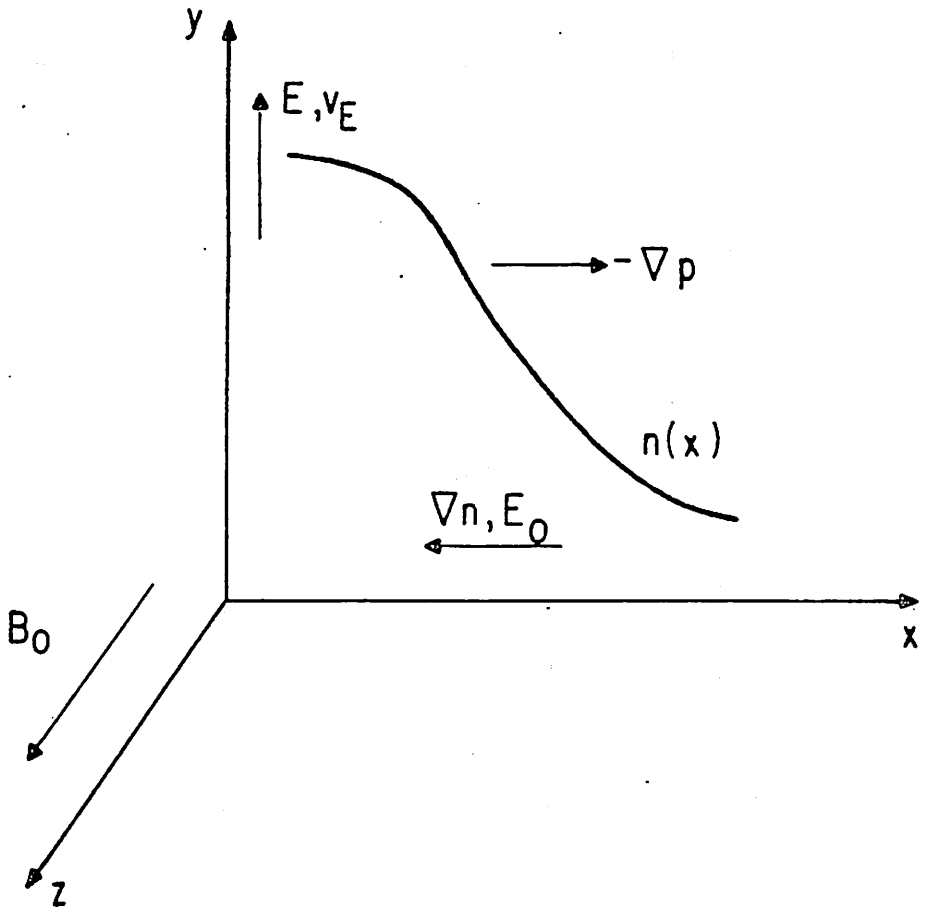

Fig. 1 Slab coordinates for lower-hybrid drift instability. Two dimensional simulations were performed in the x-y plane.

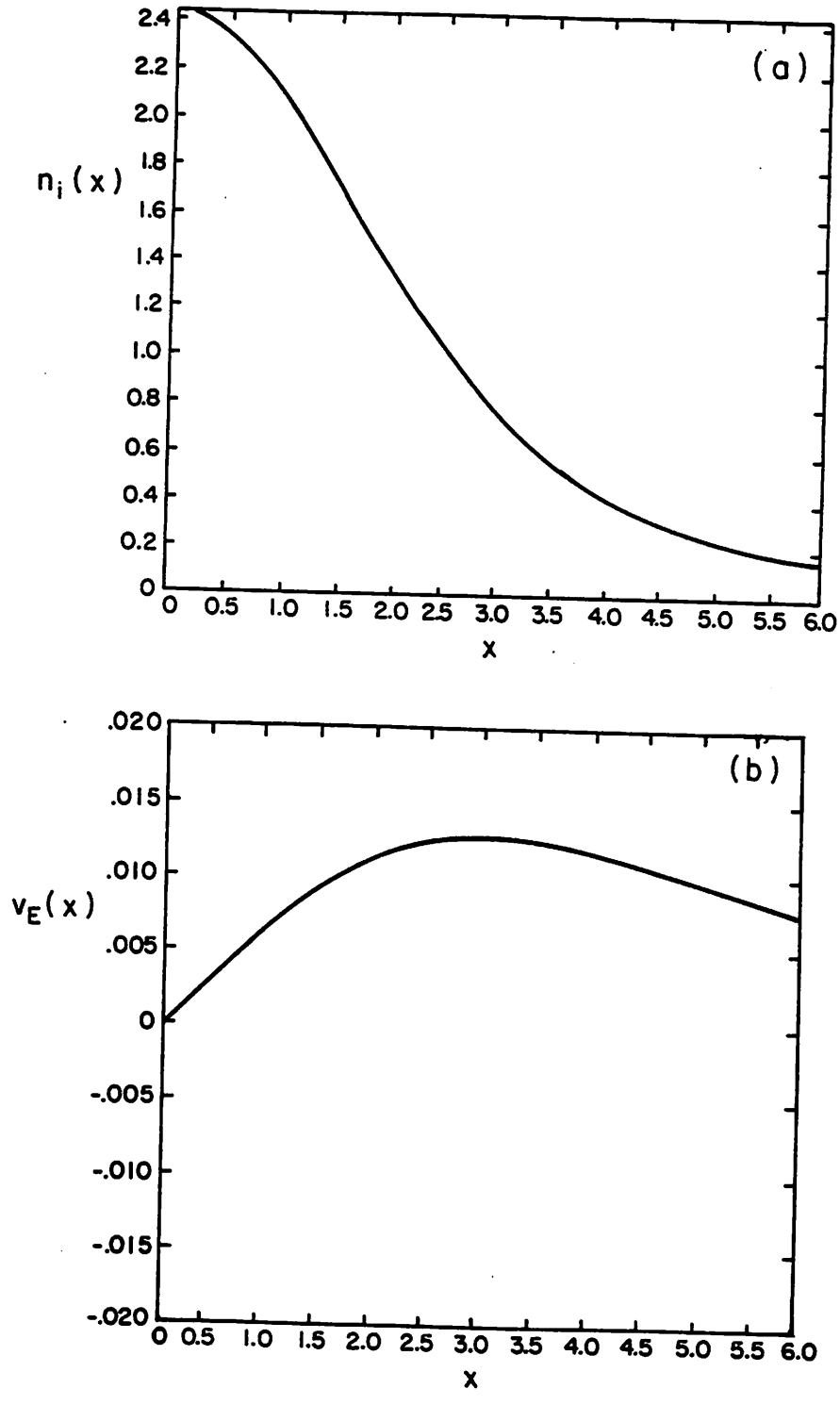

Fig. 2 Equilibrium profiles of (a) the ion density $n_i(x)/n_0$ and (b) the relative electron-ion drift velocity $v_E(x)$.

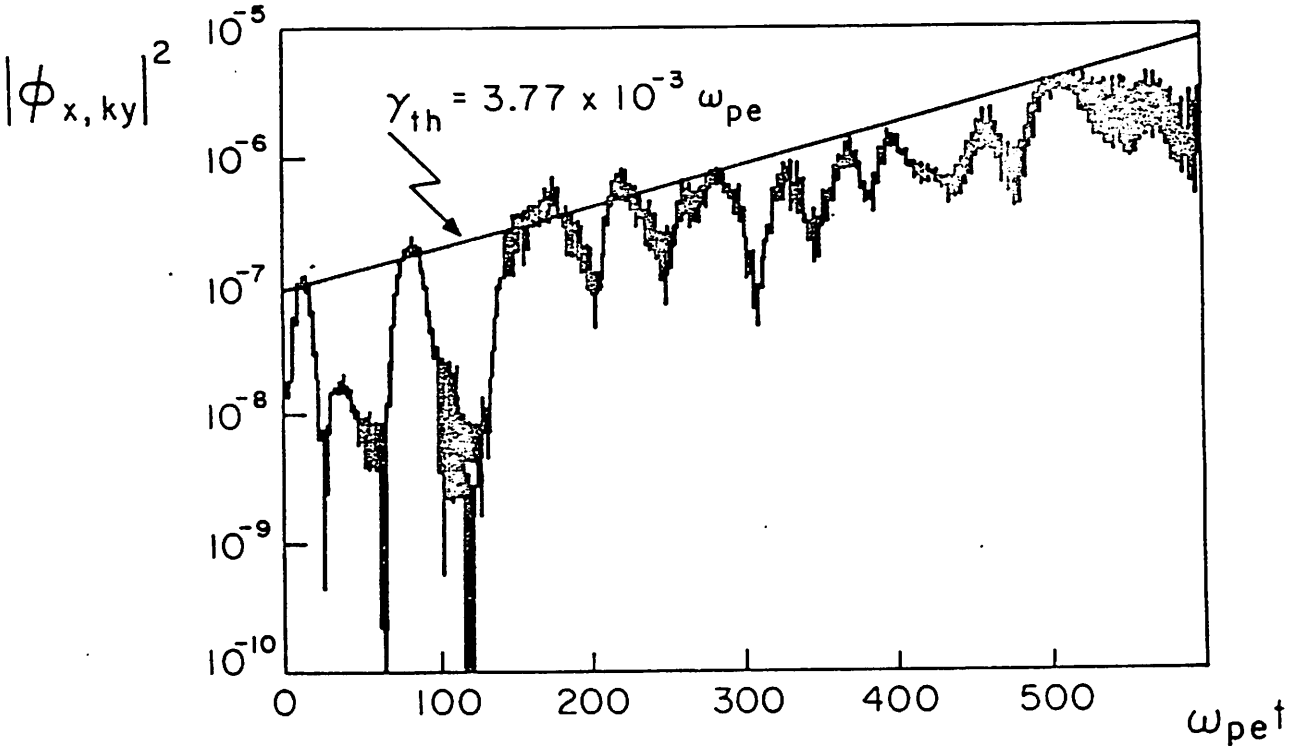

Fig. 3 History plot of the perturbed electrostatic energy of a single mode at x_0 where electrons have the largest $\vec{E}\times\vec{B}$ drift velocities. Parameters are $m_i/me=100$, $\omega_{pe}^2/\omega_{ce}^2=1$, $v_E/v_{ti}=.6$ and $T_e/T_i=0$. The theoretical local growth rate is drawn as a straight line.

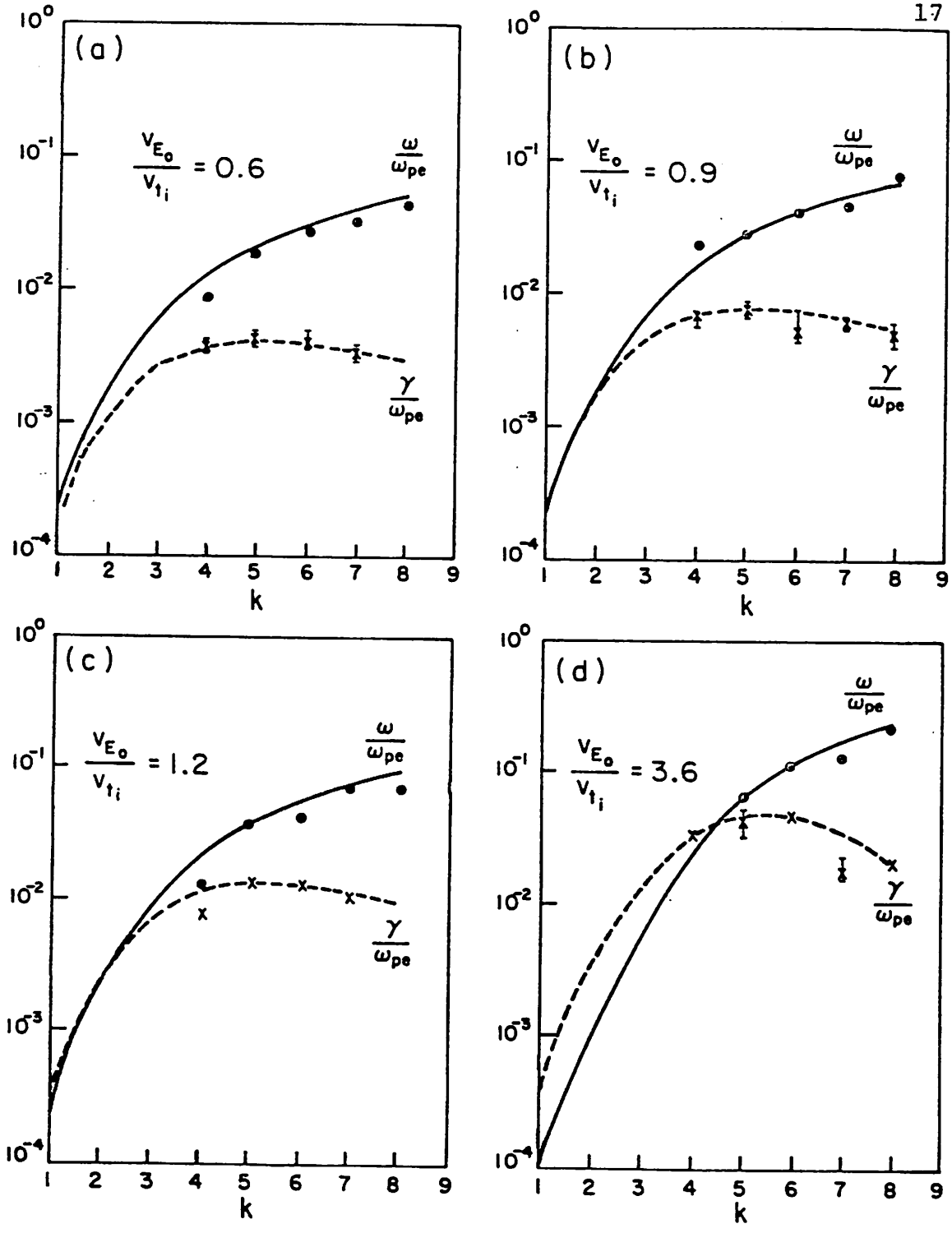

Fig. 4 Dispersion curves from local theory for the lower hybrid drift instability at where electrons have the greatest drift velocities for: $m_i/m_e=100$, $\omega_{pe}^2/\omega_{ce}^2=1$, and $v_{E_0}/v_{ti}=$ (a) 0.6, (b) 0.9, (c) 1.2, and (d) 3.6. Simulations results are denoted by dots (ω/ω_{pe}) and crosses (γ/ω_{pe}).

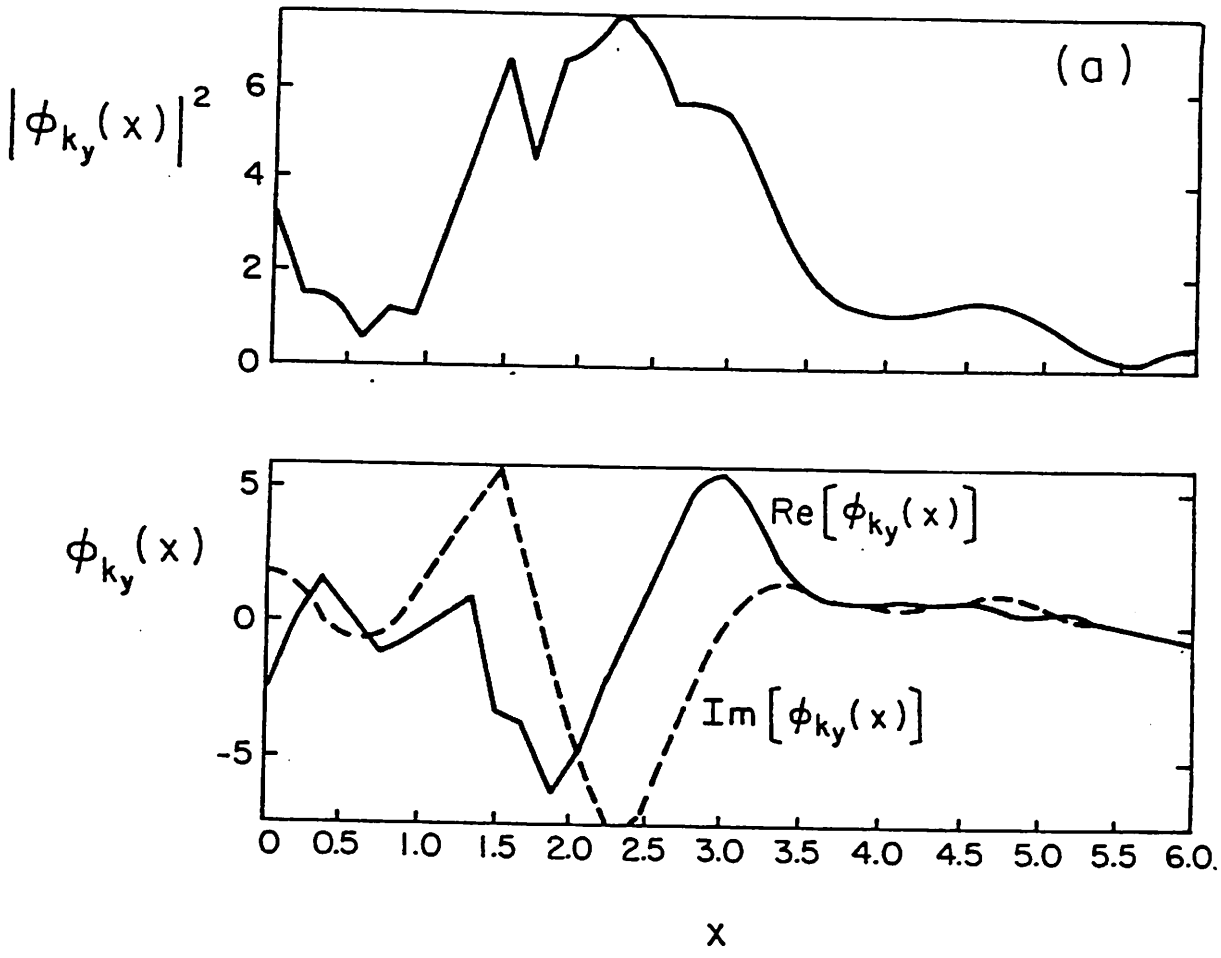

Fig. 5 (a) Simulated and (b) numerical normal mode structures of the most unstable mode for $m_i/m_e=100$, $\omega_{pe}^2/\omega_{ce}^2=1$, and $v_{E_0}/v_{ti}=0.9$. Both of them show that wave amplitude vanishes around $x=1.2$ which corresponding to the electron resonant point.

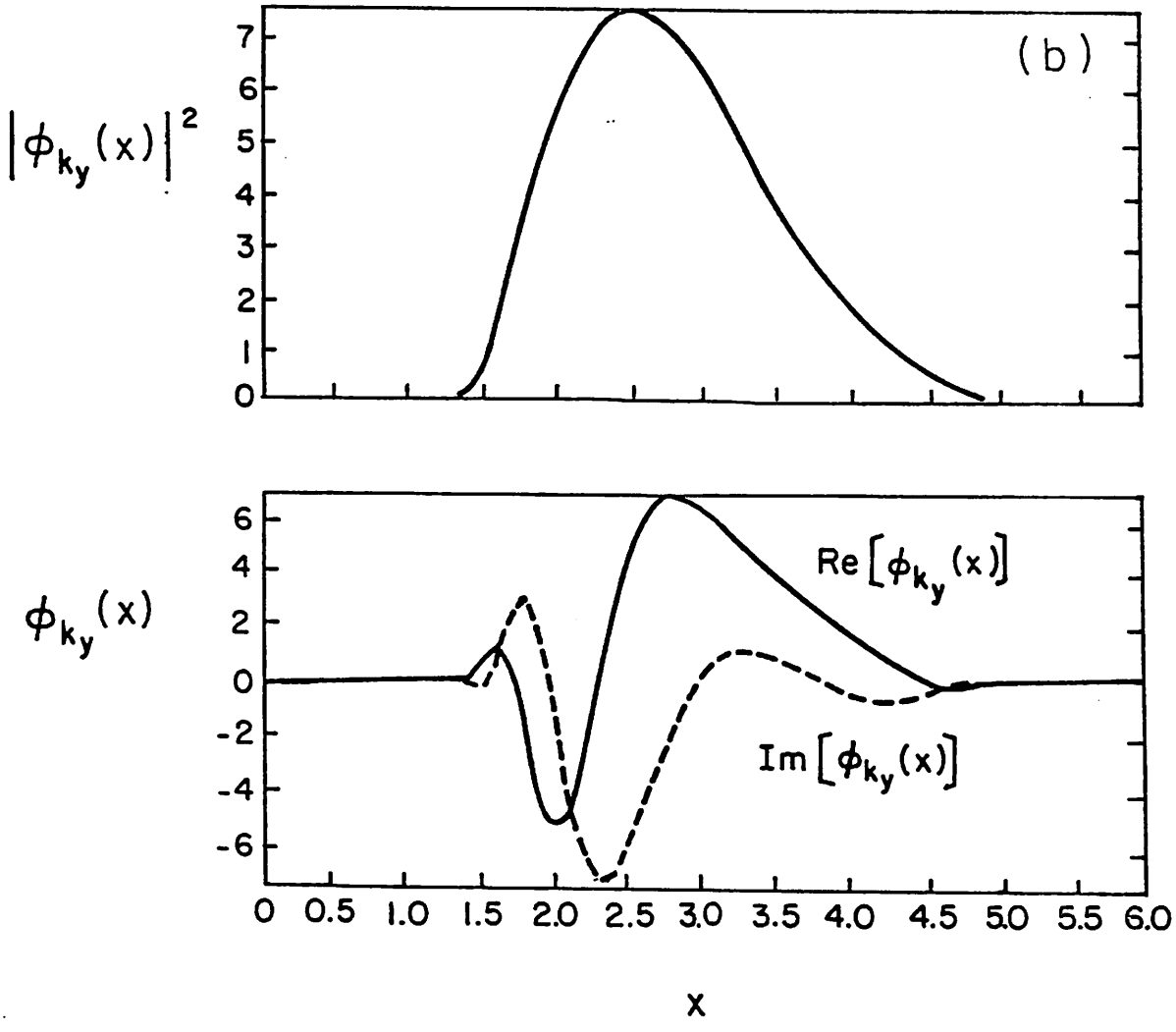
(b)
$|\phi_{k_y}(x)|^2$
$\phi_{k_y}(x)$
$\mathrm{Re}[\phi_{k_y}(x)]$
$\mathrm{Im}[\phi_{k_y}(x)]$
0 1 2 3 4 5 6 7
6 4 2 0 -2 -4 -6
0 0.5 1.0 1.5 2.0 2.5 3.0 3.5 4.0 4.5 5.0 5.5 6.0
x

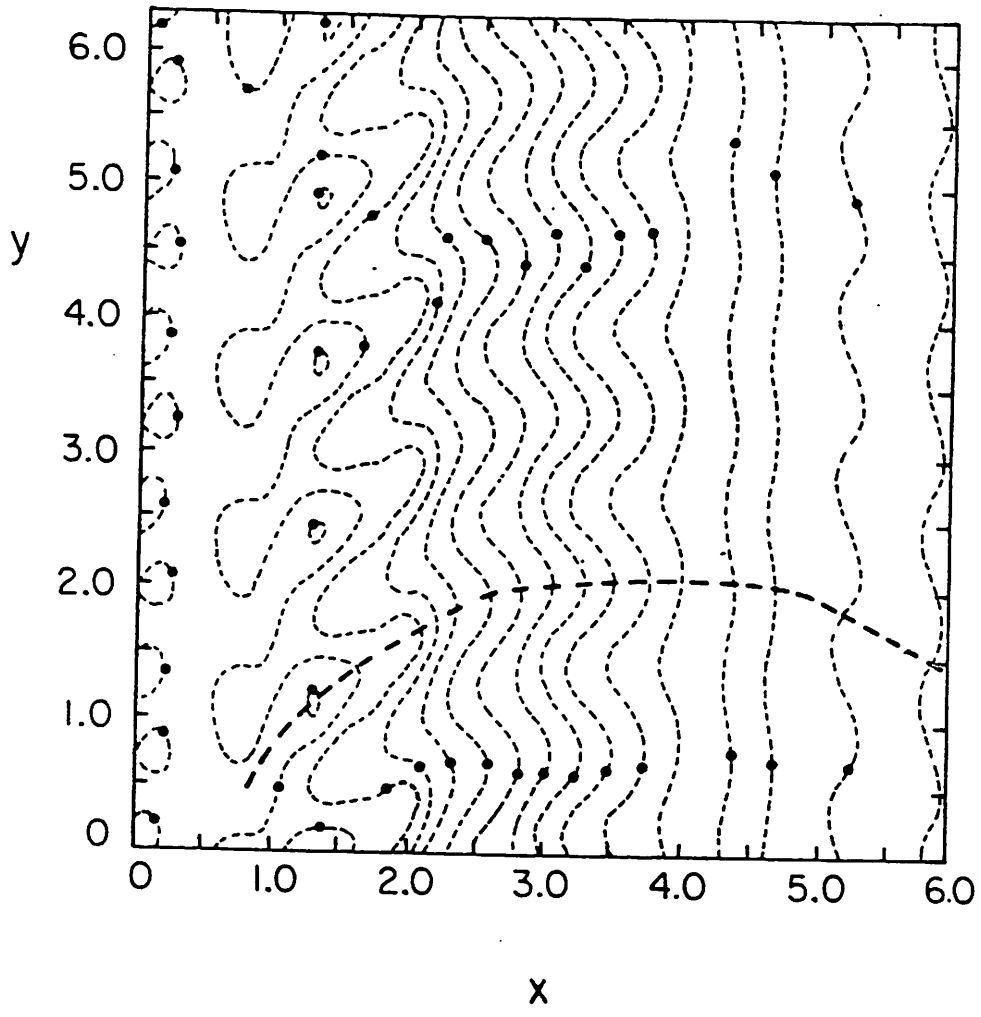

Fig. 6 Potential contours at $\omega_{pe}t$=180 for m_i/m_e=100 , $\omega_{pe}^2/\omega_{ce}^2$=1 , v_{E_0}/v_{ti}=0.9 and $k_y\lambda_{Di}$=0.707 . The dashed curve shows the wave front of the wave. Note that the vector perpendicular to the wave front is roughly at 135° for $1<x<2$ meaning $k_x \approx -k_y$. A small positive k_x component is also observed for $x>5$.

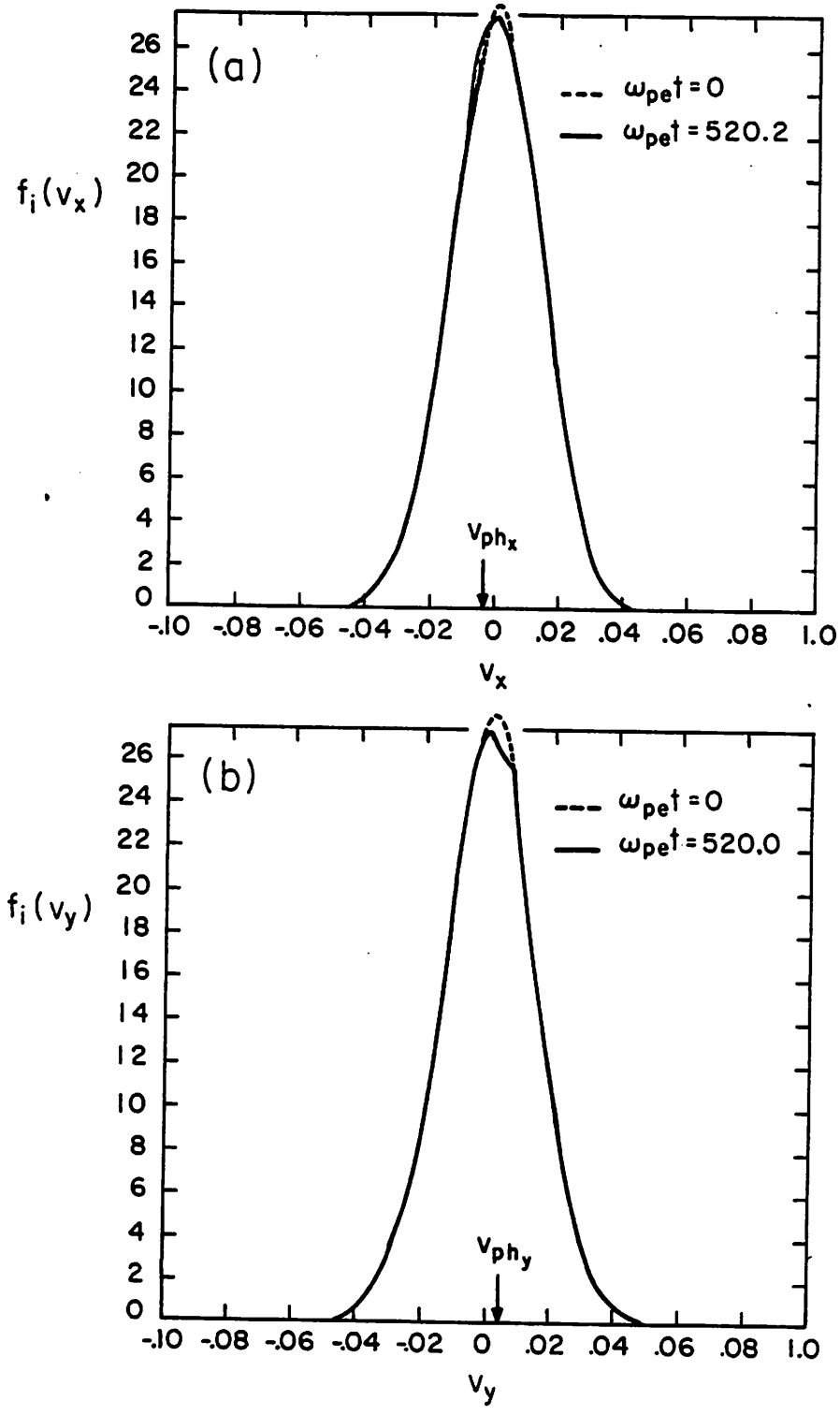

Fig. 7 Ion velocity distribution functions averaged in x over the whole system at $\omega_{pe}t=0$ (dashed curve) and after saturation (solid curve) versus (a) v_x and (b) v_y for $v_{E_0}/v_{ti}=0.6$. The small modifications at $v_{ph_x}<0.$ and v_{ph_y} imply that the wave propagates up the density gradient.

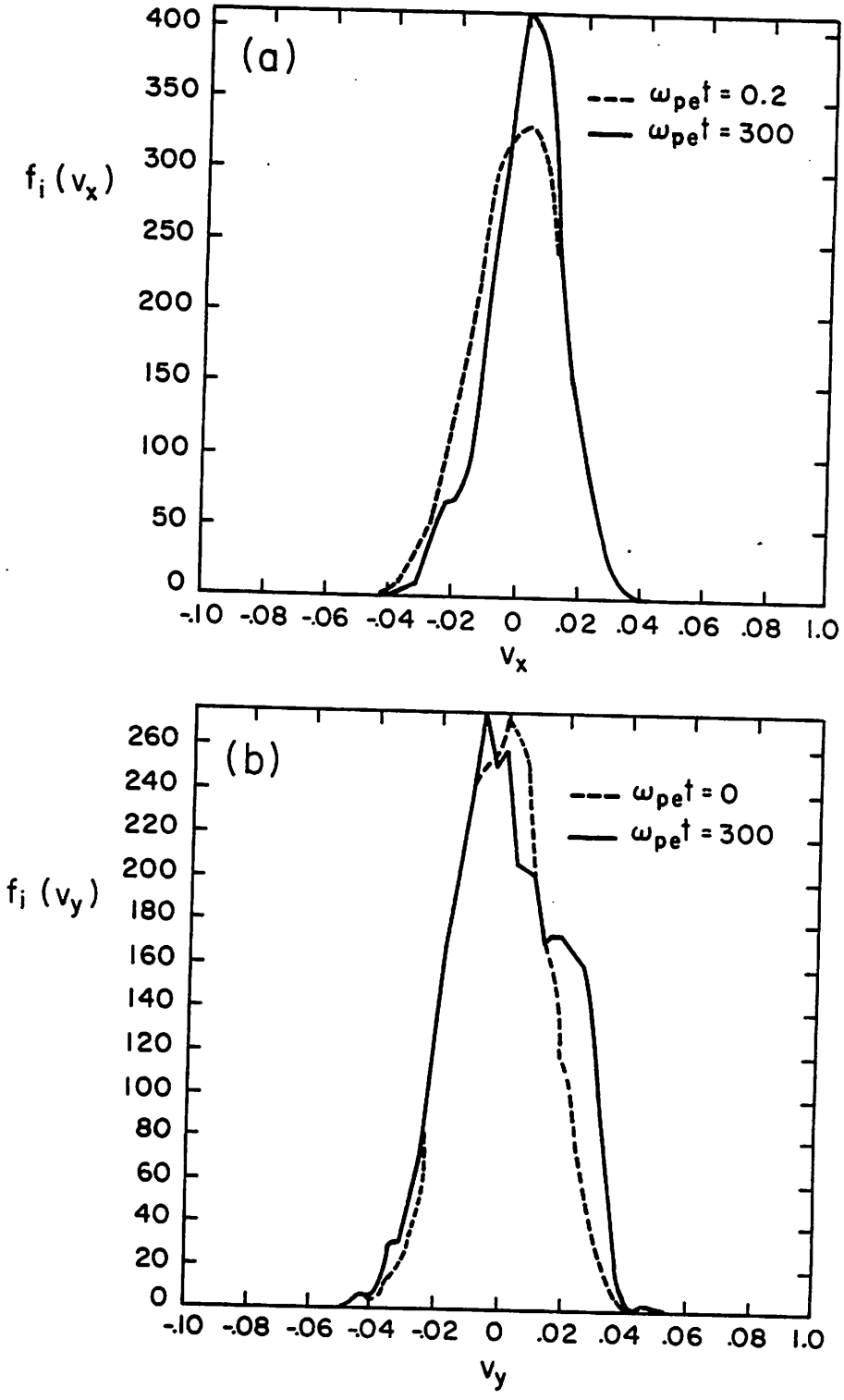

Fig. 8 Ion velocity distribution functions averaged over the most unstable region (x=2. to x=3)at $\omega_{pe}t$=0 (dashed curve) and after saturation (solid curve) versus (a) v_x and (b) v_y for v_{E_0}/v_{ii}=3.6 . Flattening in both negative v_x region and positive v_y region shows that the wave propagates up the density gradient.

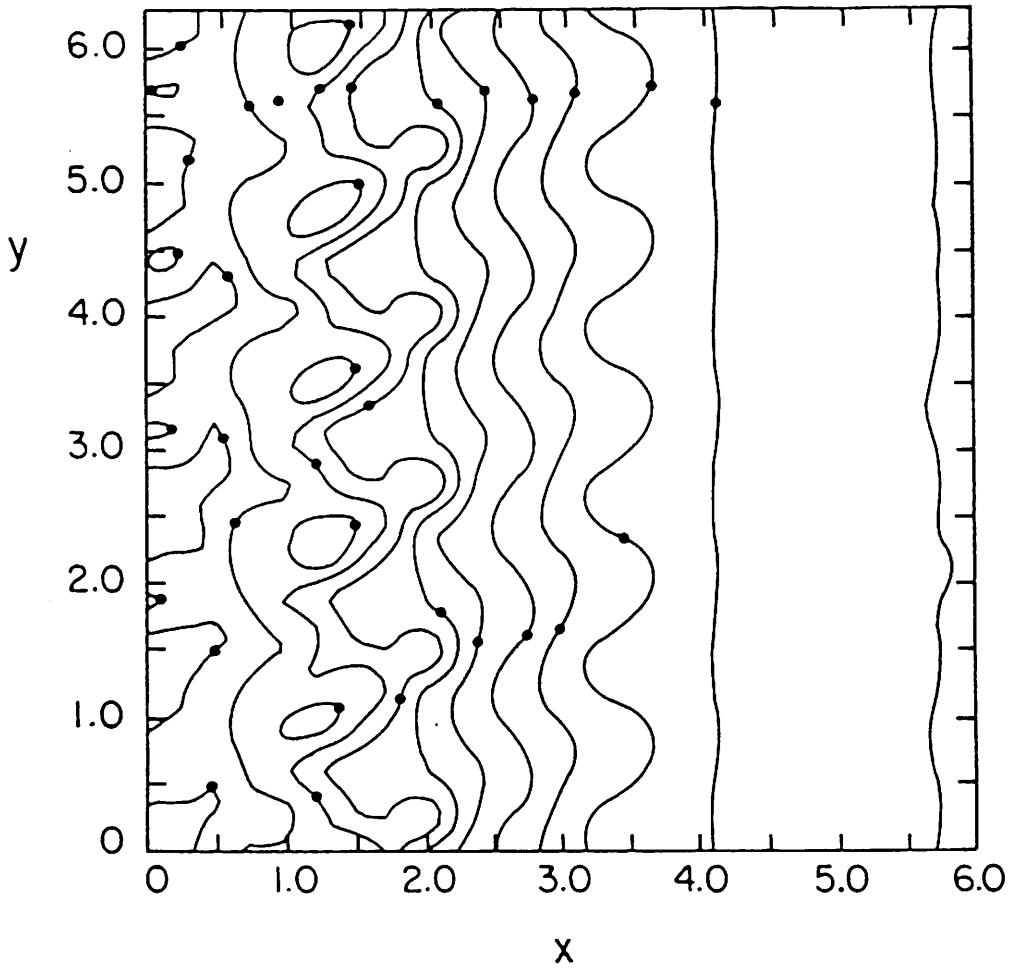

Fig. 9 Electron density contours for a single mode ($k_y\lambda_{Di}$=0.707) at $\omega_{pe}t$=179.8 with v_{E_0}/v_{ti}=0.9 . Note similarity with Fig. 6 ϕ contours, implying that electrons move along the potential contours and $\vec{E}\times\vec{B}$ trapping occurs around x=1.2 .

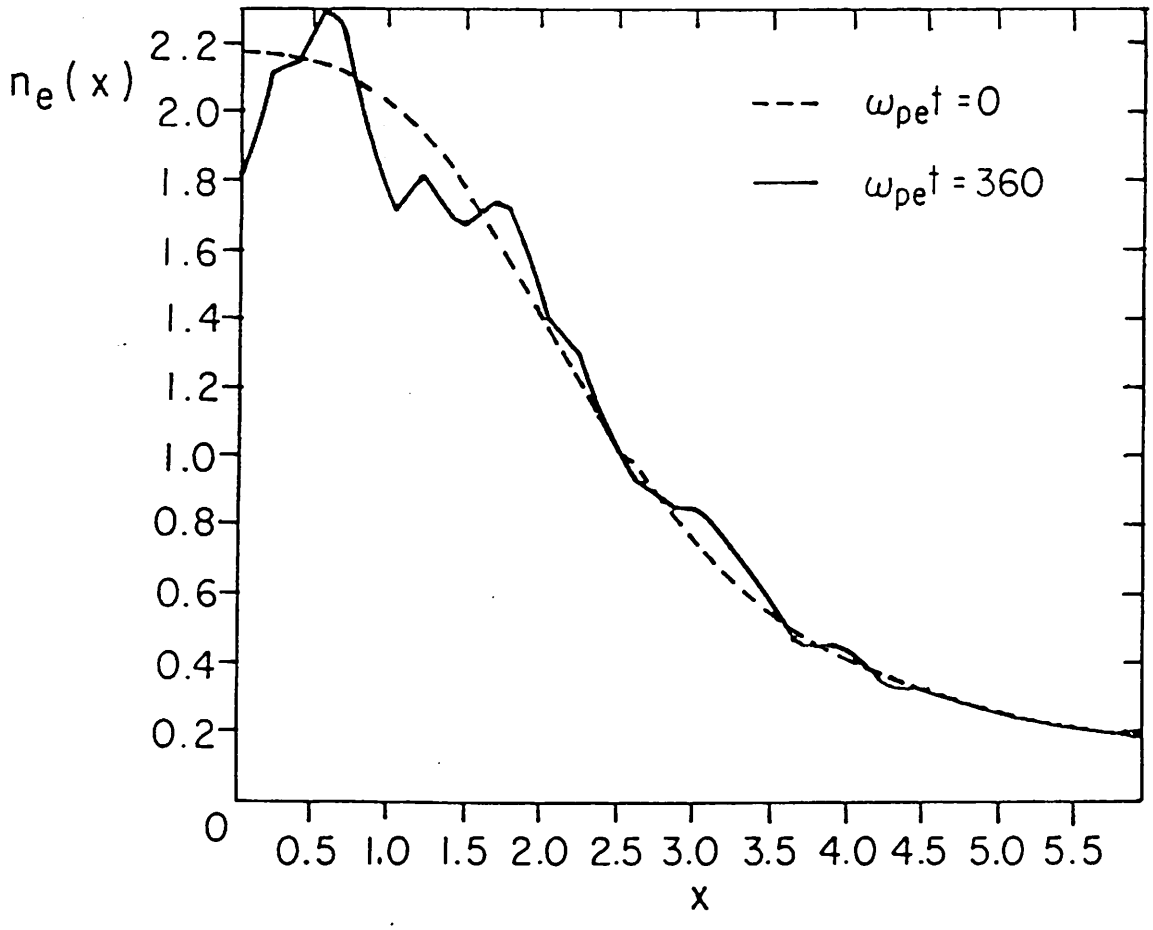

Fig. 10 Electron density profile at $\omega_{pe}t=0$ (dashed curves) and after saturation (solid curves) for $m_i/m_e=100$, $\omega_{pe}^2/\omega_{ce}^2=1$, and $v_{E_0}/v_{ti}=0.9$. The flattening around $x=1.2$ is due to electron $\vec{E}\times\vec{B}$ trapping, and the second flattening between $x=2.5$and3.0 is caused by ion quasilinear diffusion in the most unstable region.

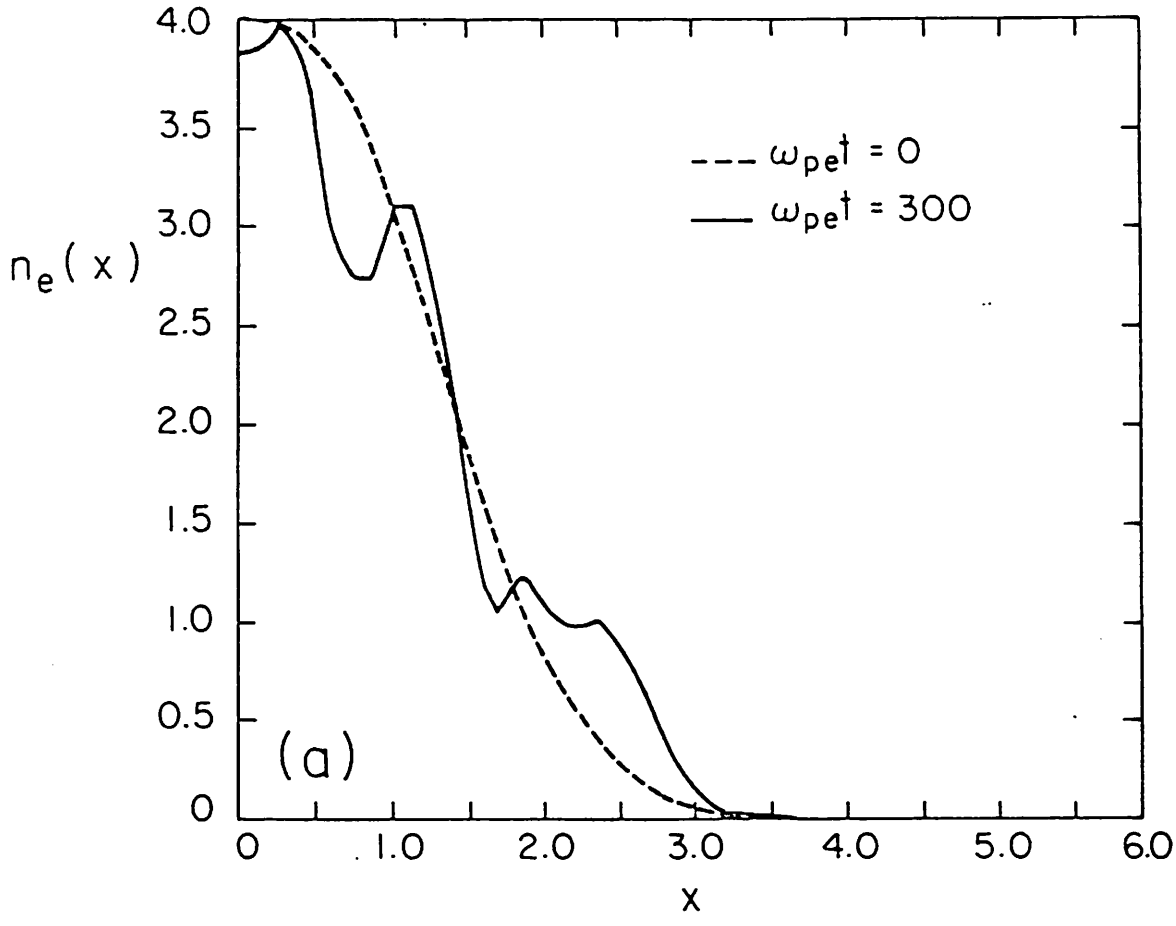

Fig. 11 Electron density profile at $\omega_{pe}t=0$ (dashed curves) and after saturation (solid curves) for $m_i/m_e=100$, $\omega_{pe}^2/\omega_{ce}^2=1$, and $v_{E_0}/v_{ti}=3.6$. Electron $\vec{E}\times\vec{B}$ trapping modifies the electron density profile around $x=1$. The density modification due to ion quasilinear diffusion is occurred between $x=2.0$and2.5 which is the most unstable region.

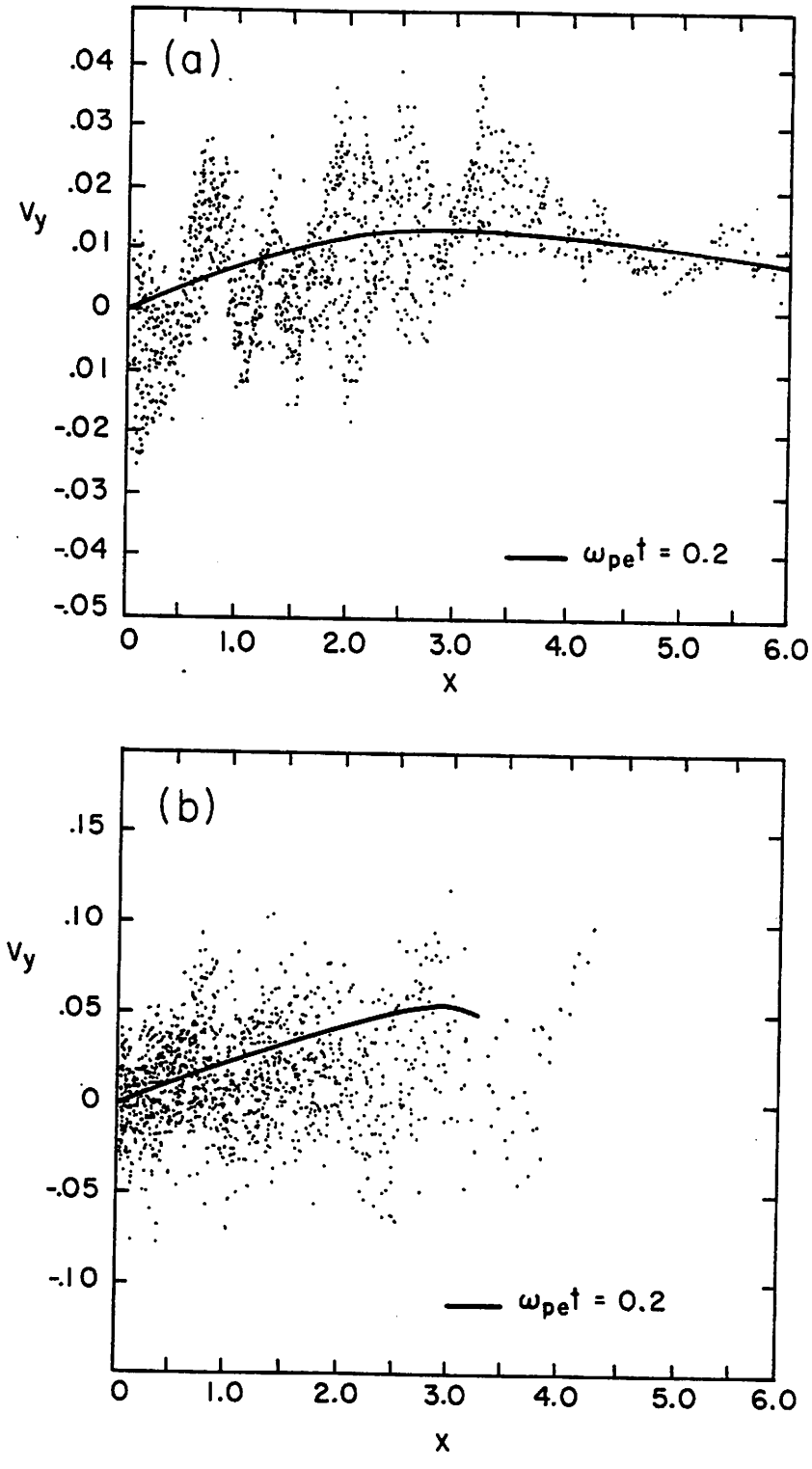

Fig. 12 Electron phase space (v_y versus x) for v_{E_0}/v_{ti}= (a) 0.9 and (b) 3.6, respectively. The initial electron temperature is zero and the initial drift velocities are given in solid curves. The averaged electron current was reduced after saturation of the wave around the largest drift velocity regions.

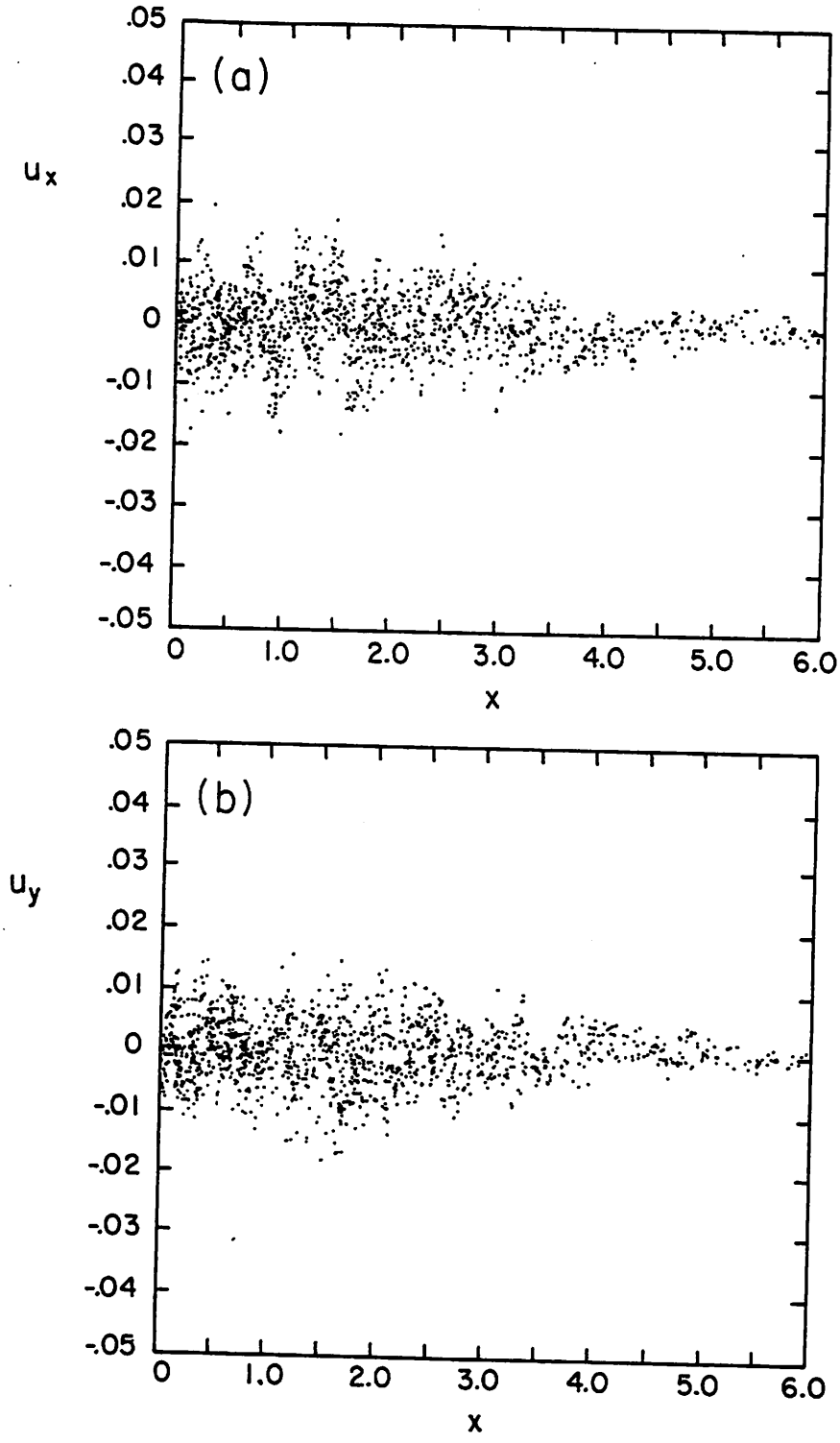

Fig. 13 Electron phase space plots after subtracing the guiding center velocity from the total electron velocity. (a) Kinetic velocity u_x versus x , and (b) u_y versus y , where $\vec{u}=\vec{v}-c\vec{E}\times\vec{B}/B^2$ and $\vec{E}$ is the total electric field in the system. The spreading in u_x and u_y shows that electrons were heated during the growth of the wave around the electron resonant region ($x\approx 1.2$), and then the heat is diffused to the whole system.

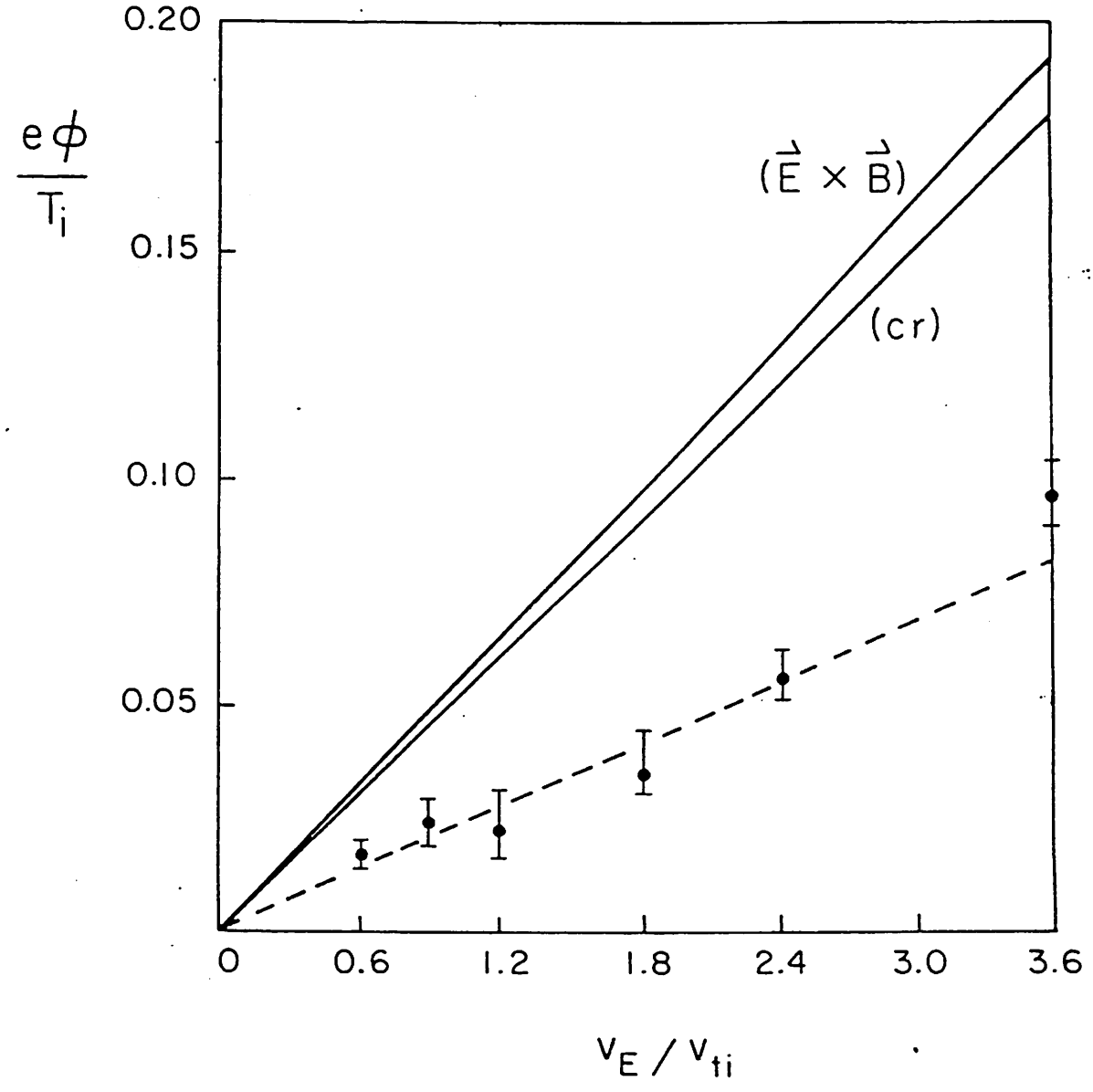

Fig. 14 Saturated lower hybrid drift mode perturbed potential $e\phi/T_i$ as function of v_{E_0}/v_{ti} for $m_i/m_e=100$, $\omega_{pe}^2/\omega_{ce}^2=1$, and $T_e/T_i=0$. Two saturation mechanisms are compared: current relaxation (cr) and electron $\vec{E}\times\vec{B}$ trapping ($\vec{E}\times\vec{B}$). Simulation results are represented by dots, roughly half that of either theory given separately.